Ambient tectonic stress as fragile geological feature

Norman H. Sleep[1]

[1]Department of Geophysics, Stanford University, Stanford, California, USA

Abstract Strong seismic waves produce frictional failure within shallow pervasively cracked rocks. Distributed failure preferentially relaxes ambient tectonic stresses, providing a fragility measure of past strong shaking. Relaxation of the regional fault-normal compression appears to have occurred within granite from 768 m down to ∼1000–1600 m depth at the Pilot Hole near Parkfield, California. Subsequent movements on the main fault have imposed strike-slip stress within the relaxed region. Peak ground velocities of ∼2 m s^{-1} are inferred for infrequent (few 1000 yr recurrence) past earthquakes from stress relaxation within the granite and from the variation of *S* wave velocity with depth in the overlying sandstone. Conversely, frequent strong shaking in slowly deforming regions relaxes shallow ambient tectonic stress. This situation is expected beneath Whittier Narrows, where strong Love waves from numerous San Andreas events repeatedly produced nonlinear behavior.

1. Introduction

Fragile geological features provide evidence of the intensity of past seismic shaking. Precariously balanced rocks are widely used in this manner [*Brune*, 2001; *Anderson et al.*, 2011]. The survival of the rocks indicates that a level of shaking (that can be calibrated) was not reached during the lifetime of the rocks. Conversely, failure of the feature, here toppling of the rocks, indicates that the level was exceeded. It is worth appraising additional possible fragile features as conditions suitable for the formation of precarious rocks are not ubiquitous and as precarious rocks are sensitive to modest levels of shaking.

The purpose of this paper is to illustrate and appraise the hypothesis that the persistence of shallow ambient tectonic stress can be used as a fragile geological feature to constrain the amplitude of past strong shaking. My methodology provides evidence on stronger levels of shaking than do precarious rocks. It is relevant to the possible rare occurrence of extreme shaking within relatively stable areas [*Hanks et al.*, 2006; *Andrews et al.*, 2007; *Anderson et al.*, 2008].

The basic physics of the hypothesis are relatively simple, yielding analytical expressions for past dynamic strain and peak ground velocity (PGV). Dynamic stresses from strong seismic waves impinge on rocks with ambient tectonic stresses. The stressed rock becomes nonlinear with sufficiently high total stress. The sum of the oscillating dynamic stresses, zero-tensor-average local prestresses, and static tectonic stresses drives coseismic anelastic strain; cracks within the rock mass do not distinguish between these remote sources of stress. Frictional failure distributed throughout the rock mass tends to relax the combined stress. Repeated failure within a rock mass during random oscillating dynamic stress thus tends to relax the ambient tectonic stress. This work follows the use of damage from cracking in shallow ambient rock as a fragile geological feature [*Sleep and Erickson*, 2014].

Conversely, knowledge of coseismic stress relaxation allows prediction of ambient tectonic stresses and comparison with observations. As a societal matter, nonlinear numerical models of strong seismic waves from San Andreas events include spatially varying ambient tectonic stresses [*Roten et al.*, 2014]. The existence of these stresses produces an apparent anisotropy with regard to which directions of Love waves propagate efficiently. In particular, models of San Andreas events indicate that high-amplitude Love waves pass through Whittier Narrows on their way to Central Los Angeles. The nonlinear behavior occurs in the upper few hundred meters, so the ambient tectonic stress at those depths in this locality is relevant.

The approach of this paper is to model the interaction of dynamic and static stresses in cracked rock to constrain when strong seismic shaking relieves ambient tectonic stresses. The formalism yields closed-form

expressions in terms of convenient variables. That is, material properties that can be measured and peak ground velocity. I begin with an outline of the well-known construct of rate and state friction and qualitatively extend the formalism to waves in the three-dimensional subsurface. I consider downhill slip on a shaken hillside as a simple illustrative numerical example. I then I apply the methodology to the Parkfield, California region to constrain the maximum amplitude of past strong shaking. I finally constrain the likely shallow tectonic stress beneath Whittier Narrows where strong shaking is frequent.

With regard to the reality of ambient tectonic stress changes within shallow hard rocks, *Nakata and Snieder* [2012a] measured the direction of *S* wave anisotropy within the uppermost few hundred meters by analyzing records from collocated borehole and surface stations. The direction of anisotropy is that expected from trench-normal compression. Furthermore, strong shaking during M_W 9.0 Tohoku-Oki earthquake of 2011 decreased the shallow *S* wave velocity at numerous stations showing that rock damage did occur [*Nakata and Snieder* [2011, 2012a, 2012b; *Sawazaki and Snieder*, 2013]. The orientation of anisotropy and the *S* wave splitting time changed at some stations. Further analysis of these data including calibration of anisotropy changes versus stress changes is beyond the scope of this paper.

2. Frictional Sliding Driven by Ambient and Oscillating Stresses

Qualitatively, the rocks beneath Parkfield and Whittier Narrows have been affected by long histories of strong seismic waves. I model failure in rocks having pervasive fractures with Coulomb friction in a typical individual event. Deformation is sliding friction on the scale of a fracture and internal friction on the scale of a seismic wave. Strong dynamic deformation takes a fracture beyond its failure limit. Once slip is underway, the combined shear traction from dynamic stress, prestress, and ambient tectonics stress on the fracture is relaxed. Over time, repeated episodes of oscillating dynamic stress systematically relax the tectonic stress. This effect can be qualitatively visualized as follows: failure is most likely when the dynamic shear traction, the prestress shear traction, and the tectonic shear traction are aligned. Slip on the crack then has the sense to relieve the ambient stress. A fracture with no ambient shear traction is further from failure than a fracture with ambient shear traction, so it is least likely to fail during random oscillating shaking.

The process is related to the concept of ratcheting where an object experiences a net rigid body motion over each frictional cycle [*Barber and Ahn*, 2013]. Low-cycle fatigue [*Lubliner*, 1990] is another related concept, where cracking during repeated strong seismic shaking progressively reduces ambient shear modulus [*Sleep and Erickson*, 2014]. Safe frictional shakedown, where oscillating stresses may bring every crack below the criterion for frictional slip [e.g., *Barber*, 2011], may apply to the rock mass once shaking has ceased until the next earthquake. I examine stress relaxation directly from shaking and reduction of the ambient shear modulus from repeated coseismic cracking in sections 4.2 and 4.3, respectively, with respect to rocks beneath Parkfield.

2.1. Rate and State Friction

I begin with the strength of pervasively cracked material at the start of strong seismic waves, beginning with scalars to introduce traditional rate and state friction. Slip on individual fractures is sliding friction. The derivation follows that of *Sleep and Hagin* [2008] and *Sleep* [2010, 2011a, 2011b, 2012], concentrating on slip in the shallow subsurface driven by strong seismic waves in the presence of residual stresses.

In terms of scalars, the instantaneous shear traction τ as a function of normal traction P on a fracture is

$$\tau = P[\mu_0 + a\ln(\varepsilon'/\varepsilon'_{\text{ref}}) + b\ln(\psi/\psi_{\text{norm}})], \qquad (1)$$

where the dominant term $\mu_0 \approx \tau/P$ represents the approximation that the coefficient of friction has a constant value for a given surface (Amontons' law), a and b are small $\sim$0.01 dimensionless constants, $\varepsilon' \equiv V/W$ is the strain rate, V is sliding velocity, W is the width of the sliding zone within the fracture, $\varepsilon'_{\text{ref}}$ is a reference strain rate, and ψ is the state variable that includes the effects of healing and damage, and the ψ_{norm} is the normalizing value of the state variable which represents transient variations of normal traction [*Linker and Dieterich*, 1992]. The term $\mu_0 - a\ln(\varepsilon'_{\text{ref}})$ is effectively one constant; $\varepsilon'_{\text{ref}}$ may be set to a convenient value; experimental data then determine μ_0. The strain rate (as opposed to sliding velocity) form of the rate and state equations originated in the work of *Ruina* [1980]. It is useful here in that the strain rate on numerous fractures within the rock mass produces a tensor strain rate averaged over rock mass volume.

Behavior of quiescent fractures between earthquakes and failure of fractures during shaking are relevant. I treat them separately for brevity to avoid the complications of a hybrid approach [*Sleep*, 2012]. During the interseismic period, the state variable on static fractures increases. The aging law represents this effect [*Dieterich*, 1979]

$$\frac{\partial \psi}{\partial t} = \frac{\varepsilon'_{ref} P^{\alpha/b}}{\varepsilon_{age} P_{ref}^{\alpha/b}} - \frac{\psi \varepsilon'}{\varepsilon_{age}}, \tag{2}$$

where t is time, ε_{age} is a strain to significantly change the state variable. The pressure term represents the effect of sudden changes in normal traction; α is a dimensionless coefficient and P_{ref} is a reference normal traction. Equation (2) applies when the strain rate in the second term is small; the state variable increases linearly with time [*Sleep*, 2012]. The slip law [*Ruina*, 1983] applies once significant sliding is underway,

$$\frac{\partial \psi}{\partial t} = -\frac{\varepsilon' \psi}{\varepsilon_{slip}} \ln \left[\frac{P_{ref}^{\alpha/b} \varepsilon' \psi}{P^{\alpha/b} \varepsilon'_{ref}} \right], \tag{3}$$

where ε_{slip} is the slip to significantly change the state variable. The derivative in (3) is 0 at steady state and the argument of the logarithm is 1. This yields that the steady state value of the state variable is

$$\psi_{ss} = \frac{P^{\alpha/b} \varepsilon'_{ref}}{P_{ref}^{\alpha/b} \varepsilon'}. \tag{4}$$

Note that the aging law (2) formally has the same steady state but this law does not apply once significant sliding is underway. It is well known that the shear traction in (1) at steady state increases with strain rate if $b < a$ and decreases if $b > a$. Fracture planes are sliding velocity strengthening in the former case and velocity weakening in the latter case. Velocity weakening is a necessary condition for gradual creep to become unstable seismic slip.

With regard to transient changes in normal traction, the shear traction in (1) at steady state sliding is independent of normal traction when $\psi_{norm} = (P/P_{ref})^{\alpha/b}$. I do not consider changes in normal traction in detail, as S waves and Love waves do not change the mean normal traction. That is, I set P_{ref} to the ambient normal traction P and $\psi_{norm} = 1$. The basic feature that strong shaking relaxes tectonic stresses carries through when normal traction fluctuates, but with more complicated mathematics. The process is then qualitatively similar to shaking a machine to unjam a stress concentration.

I solve (1) for strain rate to obtain a flow law that illustrates the conditions on an ambient crack at the start of seismic shaking,

$$\varepsilon' = \varepsilon'_{ref} \exp \left[\frac{\tau - \mu_0 P}{aP} \right] \psi_{old}^{-b/a}, \tag{5}$$

where ψ_{old} is a large value obtained from (2) if the crack has not slipped interseismically and a moderately large value in (4) if the crack has come to steady state creep. I use (2) and (5) to contrast interseismic creep behavior with behavior during strong shaking within the shallow subsurface where the velocity strengthening condition $a > b$ applies.

The shear traction τ increases gradually with time during the interseismic period from (mainly deep) processes away from the crack under discussion. Creep on the crack is most likely when the imposed interseismic stress is favorably oriented with respect to preexisting stress. Eventually, the strain rate in (5) within the crack may become large enough for slip on the crack to partially relax the shear traction on the crack. Strain rate on the crack evolves to steady state where it balances the imposed interseismic strain rate. The state variable approaches steady state in (4).

Dynamic strain suddenly imposes dynamic stress throughout the rock. The parameter a is ~0.01 and the normal traction and shear traction at failure are comparable. The strain rate increases from a trivial value to a very large one over a small (few percent) relative increase in shear traction. Once slip starts, the state variable quickly drops to a low value in (3). Slip on the crack becomes effectively unstable. Crudely, the crack either fails at a stress around $\tau = \mu_{start} P$ or it does not. (The parameter μ_{start} is the effective starting friction that includes the effect of the state variable in (5). The effective coefficient of sliding friction with a low value of the state variable is much less.)

Once crack sliding is underway, slip is comparable to that to relax the imposed dynamic strain, but the details are somewhat unpredictable. The stress drop may be near total rather than a modest fraction of the total shear traction predicted by rate and state friction. Shear heating at high slip rates weakens major faults once large earthquakes are underway [e.g., *Beeler et al.*, 2008; *Noda et al.*, 2009; *Dunham et al.*, 2011a, 2011b]. The applicability of this mechanism is doubtful with regard to small displacements on distributed cracks. The low confining pressure in the shallow subsurface may be important. Slip may transiently dilate cracks out of contact greatly reducing their strength.

Returning to data, small earthquakes driven by dynamic strain in the shallow subsurface confirm the reality of coseismic crack failure [*Fischer et al.*, 2008a, 2008b; *Fischer and Sammis*, 2009]. The largest of these events produce accelerations above 1 g [*Aoi et al.*, 2008; *Sleep and Ma*, 2008]. Cracks where the dynamic shear traction is favorably oriented with respect to prestress and tectonic stress favor preferentially. The process grades into triggering of tectonic earthquakes at greater depths [*Hill*, 2008].

With regard to a mathematical caveat, the alternative temptation to expand (5) into a Taylor series should be avoided. To illustrate, I let $\tau = \tau_{dyn} + \tau_{amp}$, the sum of the large dynamic shear traction and a smaller ambient shear traction. The strain rate is $\varepsilon' = \varepsilon'_{dyn} + \Delta\varepsilon'$, where ε'_{dyn} is the creep rate in (5) from the dynamic stress alone and $\Delta\varepsilon'$ is the change. The predicted relative change in creep rate is,

$$\frac{\Delta\varepsilon'}{\varepsilon'_{dyn}} = \frac{\tau_{amp}}{aP}. \tag{6}$$

The series usefully converges only for tiny ambient stresses where the predicted relative change is less than 1.

2.2. Application to Three Dimensions

The subsurface is three-dimensional. I present tensor formalism as a qualitative guide and as an outline to formulating numerical models. Seismic waves impose deviatoric dynamic stress $\tau_{ij}(dyn)$ and dynamic strain $\varepsilon_{ij}(dyn)$ (*ij* are tensor indexes) on a rock mass. The rock mass has ambient deviatoric stress $\tau_{ij}(amb)$. Past crack failure imposes random zero-tensor-average prestresses $\tau_{ij}(pre)$ that vary between individual cracks. These stresses resolve into shear tractions on very numerous randomly oriented cracks. Failure on an individual crack occurs when the sliding velocity in (5) becomes large.

I constrain the net anelastic strain rate in a mass of rock with pervasive interacting cracks. *Roten et al.* [2014] used a simple and computationally efficient formalism. The *Drucker and Prager* [1952] relationship uses invariants of the total stress tensor σ_{ij} and the deviatoric stress tensor τ_{ij}. The most straightforward generalization rate and state to a rock mass is that normal traction in (1–5) becomes $|P| \equiv \sigma_{ii}/3$ (compression positive), and the shear traction becomes $|\tau| \propto \sqrt{\tau_{ij}\tau_{ij}}$, normalized so that it is the shear traction in simple shear. Friction failure occurs when $|\tau| > \mu_{start}|P|$. The applicability of this these inferences to shallow rocks are a potentially testable hypothesis.

Qualitatively, failure within a rock with prestressed fractures occurs over a range of stresses with the favorably oriented fractures failing first. Residual stresses on a crack after slip subsequently become prestresses for later events. Repeated shaking and crack failure maintain zero tensor average but nonzero root-mean-square prestresses at a quasi steady state. Fractal stresses provide a useful representation of the micromechanics [*Marsan*, 2005].

As a further caveat, some fractures may experience low normal traction or even absolute tension during shaking. Shear strength is then lost. Qualitatively, near total stress drops then can occur on these cracks. For example, relationships based on invariants do not give precise representations for attenuation within a material with widely distributed noninteracting cracks that come into tension [*Jana and Chatterjee*, 2013]. An improved relationship beyond that of *Drucker and Prager* [1952] is not available for a pervasively cracked material.

To continue, the rock mass now experiences strong oscillating seismic shaking. Cracks fail within the material at the times they are favorably oriented. Slip occurs in the sense to relax the instantaneous stress. In the case of significant nonlinear failure of the rock mass, the anelastic strain near a failed crack is proportional to the sum of the elastic strains (as obtained by assuming linearity) from dynamic, ambient, and local prestress stress

$$\Delta\varepsilon_{ij} \approx \frac{1}{G}\left(\tau_{ij}(\text{dyn}) + \tau_{ij}(\text{amb}) + \tau_{ij}(\text{pre})\right), \tag{7}$$

where G is the shear modulus and $\tau_{ij}(\text{pre})$ is the local (zero-tensor-mean) prestress. The stress of failure occurs when total shear traction exceeds $|\tau| > \tau_{\text{fail}} \equiv \mu_{\text{start}}|P|$. The scalar stress local drop scales with that stress. Failure in (7) occurs most frequently and at lower dynamic stresses when the dynamic stress and local prestress are dynamically aligned with the ambient stress. There is a net bias for anelastic strain in the orientation $\tau_{ij}(\text{amb})/|\tau_{ij}(\text{amb})|$ to relax the ambient stress, as dynamic stresses and prestresses average to zero over space and time.

Equivalently, the rock mass loses information on its initial state of average ambient stress and local prestress after a sufficiently protracted strong shaking. Under external strain boundary conditions, the ambient tectonic stress relaxes toward zero. The (possibly fractal) statistical distribution of prestress and its expected average strain energy at this quasi steady state may be predictable, but the precise spatial distribution of prestress is not. Frictional failure is envisioned here as finite stress drop from starting friction. For reference, *Barber* [2011] examined the behavior of analogous systems where starting and sliding coefficients of friction are equal and provided conjectures on approach to unique steady states.

2.3. Restoration of Ambient Tectonic Stress

Tectonic processes restore relaxed ambient stresses. I obtain the time scale of this process from its kinematics. I assume that the shallow subsurface is weak and hence has little effect on the rates deep processes driving tectonic deformation. One obtains the scalar tectonic strain rate $\varepsilon'_{\text{tect}}$, for example, from the growth rates of shallow geological structures.

For comparison with the tectonic strain rate, I obtain the geological rate of strain in the shallow subsurface from coseismic stress relaxation by noting that the absolute value of strain in each failure event is $\varepsilon_{\text{fail}} = \tau_{\text{fail}}/G = \mu_{\text{start}}P/G$. By assumption, dynamic stress and strain are significant in causing the failure. So the dynamic strain at failure scales with $\varepsilon_{\text{fail}}$, with the caveat that favorably oriented fractures failure below this criterion. The fraction of anelastic strain associated with ambient stress scales as $\varepsilon_{\text{fail}}|\tau_{\text{amb}}|/(\tau_{\text{fail}}) = \tau_{\text{amb}}/G$. This slip recurs over an interval related to some multiple of the earthquake cycle time t_{quake}. (Every nearby earthquake need not produce strong shaking and an earthquake may only partially relax the ambient stress.) The long-term scalar rate strain rate is dimensionally $\tau_{\text{amb}}/Gt_{\text{quake}}$. Ambient stress relaxes dimensionally as

$$\frac{\partial \tau_{\text{amb}}}{\partial t} = -\frac{\tau_{\text{amb}}}{t_{\text{quake}}}. \tag{8}$$

This result applies when tectonic processes are not able to restore the ambient tectonic stress. Otherwise,

$$\frac{\partial \tau_{\text{amb}}}{\partial t} = -\frac{\tau_{\text{amb}}}{t_{\text{quake}}} + G\varepsilon'_{\text{tect}}, \tag{9}$$

where $\varepsilon'_{\text{tect}}$ is the tectonic strain rate. The steady state ambient stress is $G\varepsilon'_{\text{tect}}t_{\text{quake}}$. Tectonic stress essentially relaxes if this quantity is much less than τ_{fail}. In terms of strain rates, tectonic stresses relax when $\varepsilon_{\text{fail}}/t_{\text{quake}} \gg \varepsilon'_{\text{tect}}$.

3. Spring Slider on a Shallow Slope

The effective boundary conditions on a region within the Earth determine whether tectonic stresses can locally relax. As an analogy, consider a spring supporting a weight. Anelastic creep within the spring allows the weight to move downward, but the force on the spring and the stress within the spring persist. In contrast, the stress may fully relax within a spring stretched between two rigid points. Anelastic creep within the spring equivalent to the initial elastic deformation relaxes the stress.

I discuss a spring slider on a slope (Figure 1) to illustrate behavior when stresses are free to relax and when they are not. Gravity maintains a force balance. Frictional shear traction at the base of the block and an immovable buttress downslope resist sliding of the block. The sum of the forces balance
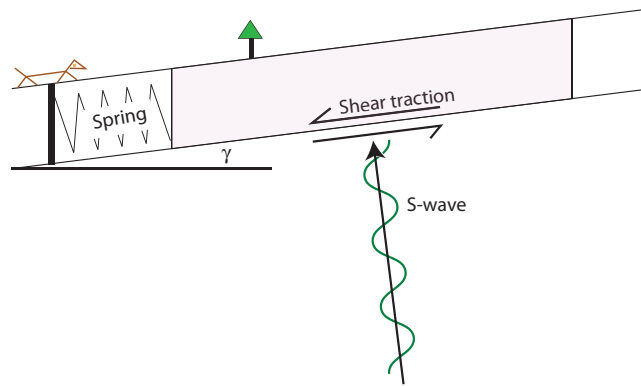
Figure 1. Schematic diagram of an idealized hill slope. Material slides systematically downhill during strong shaking. A spring represents the buttress at the base of the slope.

$$\sin(\gamma)gM = F_s + F_b = kS + F_b, \qquad (10)$$

where γ is the slope angle, g is gravity, M is the mass of the block, F_b is the force from traction at the base of the block, and the force from the spring (representing the elasticity of the buttress) is $F = kS$, where k is the spring constant and S is the displacement on the spring.

Figure 1 represents the familiar case of a weight moving down a vibrating ramp and crudely a real hill slope. In the Earth, S waves are refracted into paths perpendicular to the slope. They produce random forces on the shallow subsurface, which I represent in one dimension in the downhill direction on the block. The net forces from the wave F_w, gravity, and the spring acting act on the block,

$$F = F_w + \sin(\gamma)gM - kS_b. \qquad (11)$$

Friction on the base of the block balances this force when it is sufficient small. Otherwise, slip occurs in the direction of the net force.

I parameterize the net anleastic behavior in normalized units, so that the force on the base of the block behaves like a Coulomb stress ratio of shear traction to normal traction. The spring constant, the mass of the block, and gravity are 1. Slip occurs when the total shear traction on the sliding plane exceeds its elastic limit. Failure begins at a normalized force of $|F| > 0.5$. For greater normalized force, the displacement (change of S during a time step) is $0.1 * (|F| - 0.5)^{1.5}$. This function is arbitrary, but has the feature of being mildly nonlinear. The displacement during each time step is typically small, so catastrophic failure does not occur. Overshoot, which reverses the sign of stress on the spring, is allowed. The effects of inertia can locally cause overshoot within a real rock mass. The model does not have explicit time dependence, so it represents the combined effects of numerous earthquakes as well as the effect of continual shaking on a ramp.

I used the "rand" function in MATLAB to generate oscillations by convolving the zeroed-mean random output with the second derivative of the Gaussian $\exp(-t^2/100)$, where the units of t are in time steps. I zero-padded the ends of the time series before convolution to obtain a gradual start to shaking. I then adjusted the root mean square in the interior of the time series to either 0.35 or 0.70.

The results of a spring slider where the normalized gravitational force is 0.3 to represent a moderately steep slope are shown in Figure 2 with a flat slope for comparison. The system relaxes so that the elastic spring on rigid buttress on average supports the gravitational forces and the shear traction the base of the block is on averaged zero. That is, the normalized displacement fluctuates about 0.3 for the moderate slope and 0 for the flat slope as expected. There are periods where the block does not slide in the model with lower normalized displacement. The fluctuations are larger for the larger normalized displacement.

For comparison, I set the spring constant to zero, effectively removing the buttress and allowing the block to slide indefinitely (Figure 3). I set the normalized gravity force to 0.03 so that the net slip on the mild slope can be conveniently plotted with the random walk of the block on the flat slope. The amounts of net downhill slip and of random walk increase, as expected with the amplitude of the imposed oscillations.

Returning to the Earth, downslope movement occurs during strong seismic shaking. The uppermost tens of meters of material moves ~1 m downhill. The net effect of many earthquake cycles is a slow relatively deep landslide, called a suckung [*McCalpin and Hart*, 2003; *Sleep*, 2011a]. Thermoelastic stresses from seasonal temperature changes can have the same effect and coexist with episodic coseismic motion [*Bakun-Mazor et al.*, 2013]. Oscillating tidal stress repeatedly bring shallow cold icy with outer solar system moons to frictional failure facilitating systematic deformation driven by thermal buoyancy, that is convection (A. C. Barr and N. P. Hammond, A common origin for ridge-and-trough terrain on icy satellites by sluggish lid
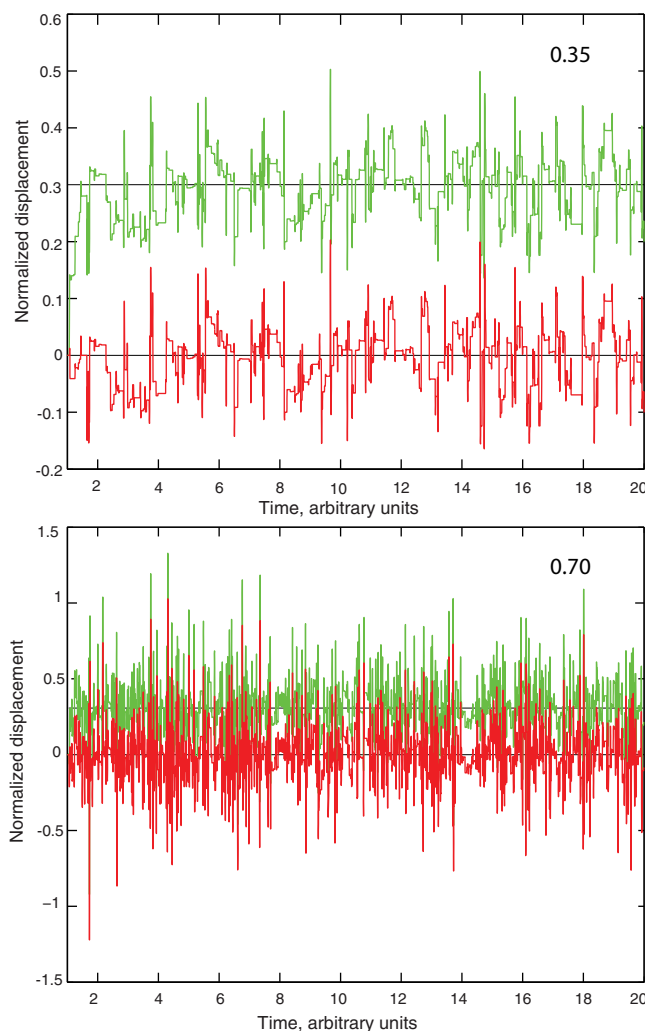
Figure 2. Displacement history for hill slope buttressed by a spring. Slip occurs so that stress on the sliding surface is on averaged relaxed. The normalized oscillating stress is either 0.30 or 0.70. Time units are 1000 numerical steps.

convection, submitted to *Icarus*, 2014). The uncommon occurrence of sackungen on slopes that are well below the angle of repose and the persistence of topographic relief in general indicate that shaking strong enough to frequently destabilize shallow slopes is relative rare [*Sleep*, 2011a]. Neither do mesas typically tend to wander laterally in random walk by repeated seismic shaking.

The models qualitatively represent some features of three-dimensional behavior of a rock mass. The time average of stress in the model is essentially the spatial average over numerous domains in the rock. If small domains are examined, there is large scatter about the average. The scatter between large domains that average many small domains is much less.

4. Application to Parkfield Pilot Hole

Geophysicists are able to measure the ambient tectonic stress within shallow rock. However, few such measurements are available. I select the Parkfield Pilot Hole as an example because both ambient stress and material properties data are available (Figure 4). Granite at 768 m depth underlies Cenozoic s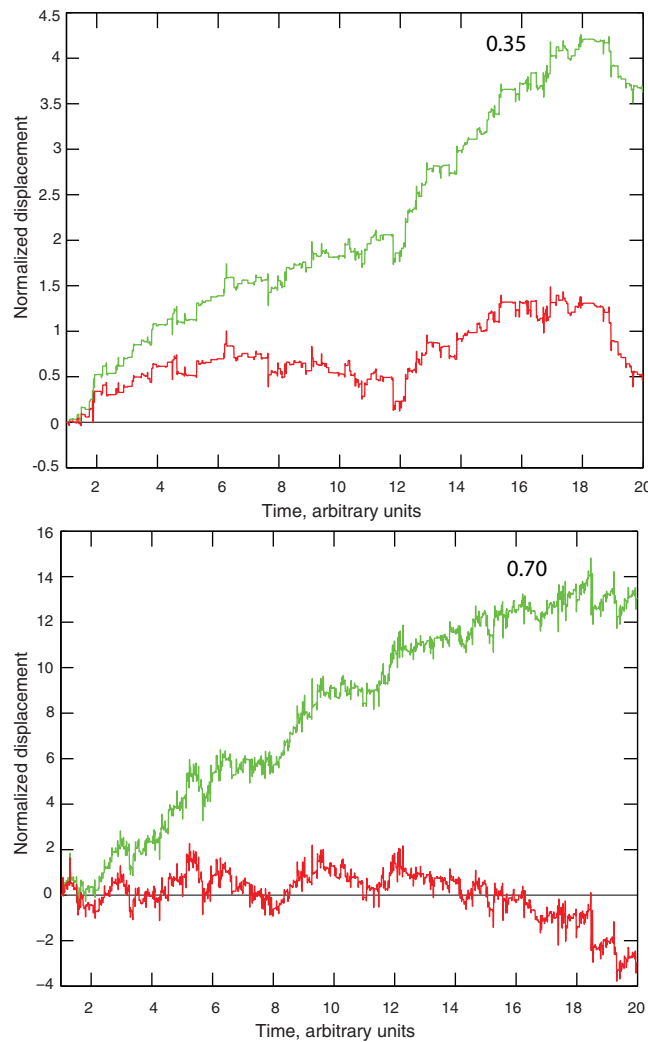edimentary rocks, mainly sandstone. Logs were collected within the granite between 775 and 2150 m depth as well as in the sandstone [*Boness and Zoback*, 2004, 2006a, 2006b; *Hickman and Zoback*, 2004, *Zhang et al.*, 2009; *Day-Lewis et al.*, 2010; *Ryberg et al.*, 2012]. The granite and the sandstone have the material property appropriate the conceptual model in section 2.3; they are pervasively fractured and hence are likely to be able to accommodate significant anelastic strains by distributed frictional sliding.

Measured stress fluctuates in a scale-independent manner in the borehole as expected from residual stresses from failure on numerous cracks. These stresses will become prestresses in future seismic events. In addition, there are systematic variations in the spatially averaged ambient stress [*Boness and Zoback*, 2004; *Day-Lewis et al.*, 2010]. The granite above ~1000 m depth exhibits stress where the axis of compression is in the orientation for strike-slip slip deformation (Figure 5). The ambient stress transitions to the regional off-fault orientation of fault-normal compression at ~1600 m depth. Note that *Zoback and Healy* [1992] found no systematic change of stress direction with depth in the Cajon borehole also near the San Andreas Fault, so I stick with Parkfield.

The site is more complicated than the simple relaxation of ambient stresses envisioned in section 2.3. Still, the Hole is 1.8 km away from the main San Andreas Fault, far enough from the fault plane that "static" vagaries in the coseismic slip during earthquakes [e.g., *Bennington et al.*, 2011] may not cause large variations in ambient stress. It is unavoidable that the granite and the sandstone are close enough to the fault that

Figure 3. Displacement history for hill slope without a buttress. Slip is systematically down the shallow slope and random walk on the flat slope. The normalized oscillating stress is either 0.30 or 0.70. Time units are 1000 numerical steps.

distributed deformation associated with the kinematics of the nonplanar fault plane has likely occurred over geological time and at a minimum produced distributed fractures and distributed finite strain. Representing repeated near-field velocity pulses as random shaking warrants a caveat. Numerical modeling shows that narrow zones of near-fault nonlinear behavior widen into broad flower structures at shallow depth [*Ma*, 2008].

4.1. Tectonic and Transient Deformation Within Stable Lithosphere

I begin with stress and strain within stable continental lithosphere to introduce the more complicated situation at Parkfield. Following *Townend and Zoback* [2000], *Zoback and Townend* [2001], and *Zoback et al.* [2002], forces from plate boundaries and from drag at the base of plates cause ambient tectonic stress. Plates act as stress guides. Horizontal forces balance on a block of midplate lithosphere. There is no horizontal shear traction at the free surface. The horizontal drag on the base of the plate is assumed to be small enough to ignore locally. The horizontal forces from normal traction σ_{xx} (compression positive) acting on imaginary vertical planes at each end of the block then balance.

For simplicity in one horizontal direction, the total normal traction integrated through the lithosphere, called the stress resultant, is conserved across imaginary vertical planes through the lithosphere. It is obtained from the depth integral of normal traction

$$\Phi_x \equiv \int_{\text{lith}} (\sigma_{xx}) dz, \tag{12}$$

where the plane is perpendicular to the x direction, σ is the stress tensor, z is depth, and the integral is from the free surface to the base of the lithosphere. In the case presented below, there is no erosion or deposition so the lithostatic pressure P_{lith} remains unchanged. The rock deforms slowly in the sense to relax the difference between the horizontal stress and the lithostatic stress. I illustrate this feature by subtracting the lithostatic pressure from the integrand in (12) to obtain a resultant that is conserved in this example,

$$\Theta_x \equiv \int_{\text{lith}} (\sigma_{xx} - P_{\text{lith}}) dz. \tag{13}$$

The horizontal strain rate ε'_{xx} is constant through the lithosphere at steady state. The shallow part of the lithosphere deforms in friction, typically under hydrostatic pore pressure (Figure 6). The stress difference, scaling with τ_{fail}, increases approximately linearly with depth and does not depend on the tectonic strain rate. Typically, fluid pressure is near hydrostatic and the stress difference increases with depth with the
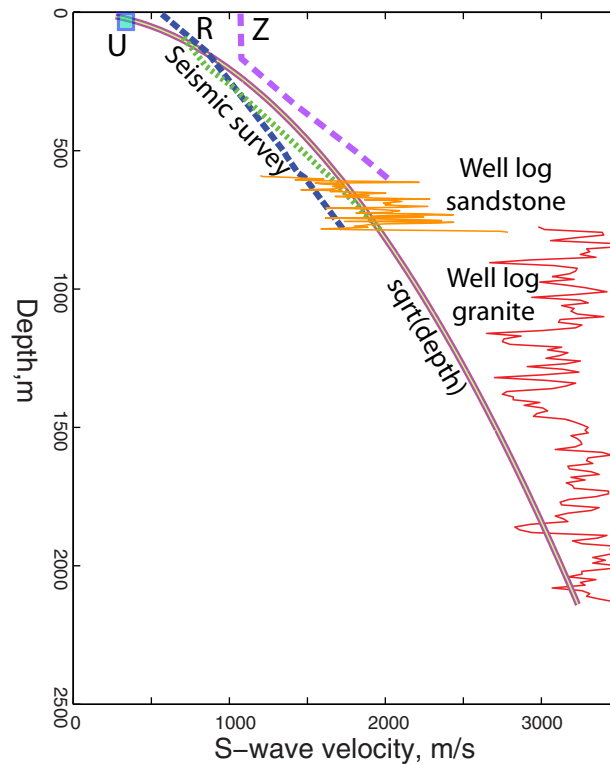
Figure 4. Seismic velocity data near the Pilot Hole as a function of depth. Well log data in granite after *Boness and Zoback* [2004] and sandstone log after *Ryberg et al.* [2012]. Seismic survey data inversions: blue-dashed and green-dotted "R" curves are two estimates by *Ryberg et al.* [2012] and purple-dashed "Z" curve is estimate by *Zhang et al.* [2009]. The tracked line is the square root of depth calibrated with the sandstone data expected from low-cycle fatigue at constant dynamic strain. The shallow seismic velocity at the nearby UPSAR array (box U) [*Fischer et al.*, 2008b] is shown, as the inversions did not have good shallow resolution. Note that S wave velocity increases slowly with depth within the granite.

apparent coefficient of friction μ_{app} between 0.6 and 1. The deep part of the lithosphere deforms in a ductile manner where the strain rate increases with the stress difference in (13). The viscosity of the material and the stress at a given strain rate decrease exponentially with depth. The deep deformation rate limits the overall rate of deformation within the lithosphere. That is, the lithosphere-wide strain rate adjusts so that the stress resultant in (13) obtained by considering rheology is that imposed by remote processes on the lithosphere.

I provide an example calculation where ambient stress relaxed down to 2 km depth where ambient stress may be measured to constrain the time scale on which midplate tectonic stresses are restored and the amplitude of shaking needed to relax them. The failure strength is $\mu_{app}(\rho - \rho_w)gz$. I ignore differences between normal, strike slip, and thrust faults for brevity. I let rock density be 2650 kg m^{-3} and water density be 1000 kg m^{-3}. The acceleration of gravity is 9.8 m s^{-2}. I assume 0.8 as a generic value of the apparent coefficient of friction. The failure stress τ_{fail} is 26 MPa. The failure strain ε_{fail} is $3\tau_{fail}/8G$, 0.2×10^{-3}. (The shear modulus $G = \rho\beta^2$ is here 4.24 GPa for S wave velocity β of 4000 m s^{-1}. I retain insignificant digits where it may

aid in following the calculations. The formula applies for strain in a sheet with Poisson's ratio of 0.25 [e.g., *Turcotte and Schubert*, 2002, p. 114].)

Rock within stable regions is typically near frictional failure and in the orientation of regional ambient tectonic stress down to several kilometers depth [e.g., *Brudy et al.*, 1997]. A useful lower limit on the typical interplate strain rate can be obtained from observations that the deep and shallow orientations of stresses in boreholes are similar. The orientation and magnitude of the stress resultant in (13) would change after a reorganization of plate motions. I illustrate a kinematic time scale to restore ambient stress difference in (13) throughout the crust starting from zero tectonic stress difference. Initially, the plate-imposed stress resultant is supported elastically throughout the lithosphere. The elastic strain produces stress differences well below those of frictional failure except at very shallow depths. The deep lithosphere creeps in a ductile manner and the stress difference relaxes in the deep part of the ductile layer. Lithosphere-wide strain produces imposes elastic strain in the shallow crust. As shallow crustal strain continues, the depth of frictional failure moves downward eventually reaching the zone of ductile creep. Deformation continues at quasi steady state until the next reorientation of plate-wide stress. Plate-wide stress reorients on the scale or tens of million years, so the lithosphere needs to approach to steady state over that time interval if the orientation of stress in fact is independent of depth within the lithosphere.

For an example related to coseismic stress relaxation, I consider the related time scale after strong shaking has relaxed the stress difference within the uppermost crust to depth Z_R (Figure 6). The stress difference increases somewhat through the remaining lithosphere to maintain the imposed stress resultant. The maximum stress and the depth to it increase somewhat to τ_{new} and Z_{max} (Figure 6). The increased stress
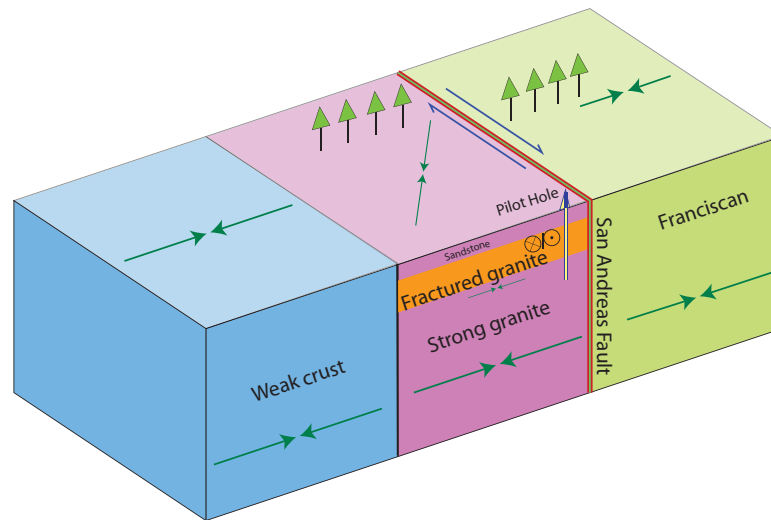
Figure 5. Schematic three-dimensional diagram through the Pilot Hole. The regional stress is approximately fault-normal compression. Creep in the deep crust maintains this stress. The stress within shallow fractured granite is that associated with strike slip. Strong shaking within the shallow granite relaxed the fault-normal tectonic stress. Movement along the fault restored the strike-slip stress. The geological structure is greatly simplified.

difference within the ductile layer speeds up the strain rate. Creep in the deep lithosphere restores the ambient stress in the relaxed depth interval. The shallow material reaches frictional failure from top down to depth Z_T. Steady state is restored when $Z_T = Z_R$.

I continue kinematically with the ambient strain rate. *Zoback et al.* [2002] and *Sleep and Zoback* [2007] obtain $\sim 3 \times 10^{-19}$ s^{-1} (10^{-11} yr^{-1}) as an upper limit for the stable interiors of cratons. With that rate, it takes 20 Ma to produce 0.2×10^{-3} strain to restore the ambient stress at 2 km depth. A more sophisticated model in Appendix A includes the nonlinear dependence on ductile creep rate on stress difference. This modification has little effect on this estimate.
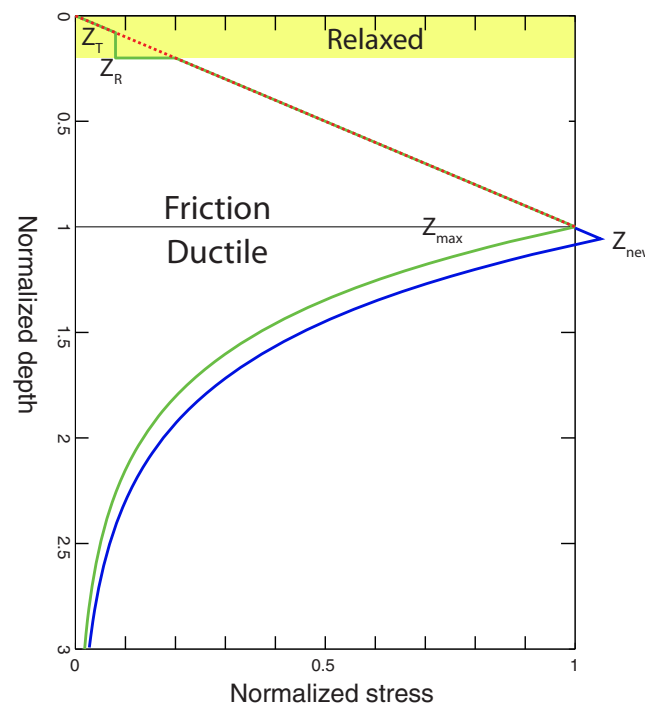

Figure 6. Schematic diagram of the stress difference through the lithosphere. The upper lithosphere fails in friction and the stress increases linearly with depth. The deep lithosphere fails in a ductile manner and the stress decreases linearly with depth. Relaxation of the stress in the shallow subsurface is balanced by an increase of stress in the lower lithosphere that results in more rapid ductile creep. Afterward, the stress at very shallow depths follows the frictional line, but the stress at the base of the relaxed zone has not yet been restored.

Returning to strong seismic shaking, oscillating dynamic strain is comparable to ε_{fail}. The particle velocity at this strain $\beta\varepsilon_{fail}$ is 2.4 m s^{-1}. It is not a major epiphany that S waves of this amplitude do not typically strike stable continental crust. It is useful, however, that the time scale to restore ambient tectonic stress is millions of years.

4.2. Tectonic and Transient Deformation Near Parkfield

The stress and strain fields near Parkfield are complicated by the different behaviors of various geological terrains and by slip on the San Andreas Fault (Figure 5). Ambient stress is approximately fault-normal compression away from the fault plane [*Boness and Zoback*, 2004, 2006a, 2006b; *Chéry et al.*, 2004; *Townend and Zoback*, 2004; *Hickman and Zoback*, 2004; *Day-Lewis et al.*, 2010], rather than at the angle to the fault expected from strike-slip deformation. In terms of geological features, the region deforms with folds and faults accommodating fault-normal compression as expected from this stress field with a rate of $\sim$6 mm yr^{-1} over the $\sim$120 km width of the

belt [*Page et al.*, 1998]. The average geological strain rate is 5×10^{-8} yr^{-1}; the strain rate is less than this within the region underlain by granite (including the Pilot Hole).

I begin with a semiquantitative discussion of fault-normal deformation. Shallow rocks in this region deform by friction, stress differences for frictional sliding accommodate much of the stress resultant in the lithosphere (13). The deep crust is readily flows in a ductile manner, but the rate is slow beneath the granite. Long-term plate rates outside the deforming zone to some extent impose the overall deformation rate.

I use generic material properties from the Pilot Hole near 1 km depth to estimate strain at frictional failure and the time to restore ambient stress with relevant material properties are reasonably constrained in round numbers. The density is 2600 kg, the water table is shallow, the S wave velocity is 3000 m s^{-1} [*Boness and Zoback*, 2004], and apparent coefficient of friction of 0.8. The frictional failure stress is 12.4 MPa and the compressional failure strain is 0.2×10^{-3} and the shear failure strain is 0.5×10^{-3}. It takes 4000 yr for the regional strain rate of 5×10^{-8} yr^{-1} to produce the compressional strain. I use $\sim 10^4$ yr for further calculations to account for the inference that the geological strain rate with the granite is less than the regional rate.

The fault slips at $\sim$30 mm yr, which is faster than the distributed fault-normal compression rate. Yet the fault is weak in the senses that stress with the orientation of strike slip does not dominate the regional stress field and friction on the fault does not liberate much heat. The theory of dynamic rupture explains these observations [*Beeler et al.*, 2008; *Noda et al.*, 2009; *Dunham et al.*, 2011a, 2011b]. The ambient shear traction on much of the fault plane is low $\sim$10 MPa, but heterogeneous. Seismic slip begins at a high shear traction nucleation patch at several kilometers depth. The deep fault plane is velocity weakening in rate and state friction $b > a$. Dynamic rupture becomes unstable. High shear tractions associated with a coefficient of friction of $\sim$1 occur at the rupture tip. Shear strain dissipates energy at the rupture tip into heat. Fluids in the fault slip zone expand and the difference beneath fluid pressure and normal traction of the fault drops to a low value. Alternatively, the material on the fault plane melts. Both of these processes greatly reduce the instantaneous coefficient of friction to below 0.1. Most of the slip occurs over at this low coefficient of friction and overall little heat is dissipated on the fault plane. The average stress drop is near the preevent average shear traction of $\sim$10 MPa, but the shear traction and slip after the event are heterogeneous. The event leaves some high shear traction patches in its wake that become nucleation zones for future events.

The rupture dynamically propagates into the uppermost few kilometers of the fault plane. On average, deeper processes on the rupture plane impose the shallow slip. Frictional failure away from the rupture tip occurs at relatively low shear tractions that do not generate much heat. In addition, the shallow fault plane is typically velocity strengthening with $a > b$. Relatively little shallow slip compared with deep slip occurred during the 2004 event [*Bennington et al.*, 2011]. Patches of low shallow slip catch up to the overall plate rate by slow aseismic creep and by having more slip during subsequent earthquakes.

The net effect is that the shallow seismic zone is near to strike-slip frictional failure. I obtain the scale time to restore this stress from kinematics. The averaged static strain $\sim 0.1 \times 10^{-3}$ in a single event scales with the ratio coseismic slip $\sim$1 m to the depth $\sim$10 km of the seismic zone. It takes $\sim$5 events to restore a strain of 0.5×10^{-3} to bring material at 1 km depth to failure or equivalent 5 m of displacement. This occurs in 170 years.

Now consider ambient stress relaxed by strong seismic shaking. Earthquakes on the fault restore this stress in $\sim$100 years while fault-normal deformation restores the stress in the much longer time of $\sim 10^4$ years, given that the Pilot Hole is underlain by slowly deforming granite. The ambient tectonic stress will have strike-slip orientation if it has been relaxed by shaking sometime in the last $\sim 10^4$, but has not been relaxed any time during the last $\sim$100 years.

It is unlikely, however, that shaking relaxes the ambient tectonic stress every $\sim$100 years. The relaxation of stress produces anelastic strain comparable to the preexisting elastic strain 0.5×10^{-3}. Relaxation of this strain across the $\sim$2 km from the fault to the Pilot Hole would produce 1 m of displacement very 100 yr with a rate of 10 mm yr^{-1}. This deformation if repeated at that interval would accommodate a significant fraction of the plate motion. Over geological time, it would have extensively deformed the rocks between the fault and the Pilot Hole. Relaxation of ambient stress near the Pilot Hole on the time scale of once in few 1000 years is more acceptable. A few tenths of millimeters per year of fault parallel slip would not be

readily apparent in geodetic studies, nor from geological relations in this complicated area. For reference, the vertical exhumation rate at the Pilot Hole over the last 4–8 Ma is 0.1–0.2 mm yr^{-1} [*Blythe et al.*, 2004].

Note that one would record little coseismic surface deformation with a geodetic study from relaxation of shallow ambient stress. The shear modulus of shallow rock is typically less than that of deep rock. To the first order, the deep stiff rock imposes strain and displacement boundary conditions on the shallow rock. Equivalently, the effective seismic moment from stress relaxation is $G\varepsilon$ times the volume over which it occurs. The moment is small because the shallow shear modulus is much less than that at depth.

I retain the material properties for the granite to estimate the level of past shaking. The transition to regional fault-normal stresses occurs between ~1000 and ~1600 m depth [*Hickman and Zoback*, 2004]. The dynamic stress in an *S* wave needs to be 12.4–19.8 MPa for failure and is $\rho\beta V_D$ where V_D is the dynamic particle velocity. The computed peak ground velocity (PGV) is 1.6–2.6 m s^{-1}. This quantity is linearly proportional to the assumed coefficient of friction and to the assumed transition depth. To avoid implying spurious precision, PGV of ~2 m s^{-1} was reached within the upper granite at the Pilot Hole. PGV did not reach recently this amplitude farther away from the fault where fault-normal ambient stress is observed.

For reference, the maximum observed PGV near the fault was 0.76 m s^{-1} in the 1966 Parkfield event [*Housner and Trifunac*, 1967] and 0.83 m s^{-1} in the 2004 event [*Shakal et al.*, 2006]. The estimated PGV is comparable to that obtained from stations near other major strike-slip earthquakes. The observed PGV was 1.8 m s^{-1} at 3 km from the 2002 Denali fault trace [*Ellsworth et al.*, 2004]. *Anderson* [2010] tabulates several other examples for PGV above 1 m s^{-1} for strike-slip faults.

A societal implication is that the Parkfield segment participated in major San Andreas events with ~5 m of slip (as in the 1857 Fort Tejon event) to the south recurrence time scale shorter than 10^4 yr. It is conceivable that some of these large events propagated into the creeping zone north of Parkfield. Measuring the ambient stress especially within granite at modest depths would constrain whether past strong shaking from rupture through the creeping zone has actually occurred.

4.3. Rock Damage From Repeated Strong Seismic Near Parkfield

I apply the concept of ambient rock as a fragile geological feature to show that ~2 m s^{-1} PGV is reasonable at the Pilot Hole. Frictional failure during strong shaking produces cracks that lower the ambient shear modulus. Self-organization of the shear modulus can occur where shaking imposes essentially strain boundary conditions [*Sleep*, 2011b; *Sleep and Erickson*, 2014]. In the case of a near-field velocity pulse, the wave propagates laterally with a phase velocity c related to the *S* wave velocity of rocks at depth. The dynamic strain is $\varepsilon_D \approx V_D/c$. The local dynamic stress is $\tau_{dyn} = \varepsilon_D G = V_D \rho \beta^2/c$. Frictional failure occurs when this stress exceeds the frictional strength $\mu_{start}(\rho - \rho_w)gz$, where for brevity the water table is shallow and the densities are constant with depth. That is at failure,

$$\tau_{dyn} = \left(\frac{V_D}{c}\right) G_{fail} = \tau_{fail} = \mu_{start}(\rho - \rho_w)gz. \tag{14}$$

At a given PGV, the shear modulus for failure is increases linearly with depth,

$$G_{fail} = \beta_{fail}^2 \rho = \left(\frac{c}{V_D}\right)\mu_{start}(\rho - \rho_w)gz, \tag{15}$$

where β_{fail} is the shear wave velocity at failure. The shear wave velocity can be measured remotely and is hence more frequently available than the shear modulus. Solving for *S* wave velocity at failure yields that

$$\beta_{fail} = \left(\frac{V_D}{c}\right)^{-1/2}\left(\frac{\mu_{start}(\rho - \rho_w)g}{\rho}\right)^{1/2}z^{1/2}. \tag{16}$$

The term within the first bracket in (16) is dynamic strain. A smaller PGV is required to break stiff rocks than compliant rocks in (15). Provided that the second bracket does not change much, the *S* wave velocity within the depth range of damage is predicted to increase with the square root of depth in (16).

I explain self-organization to the status in (15) starting with initially stiff rocks, such as granite and exhumed sediments at the Pilot Hole, and illustrate the effects of repeated shaking (Figure 7). Initially, the shear modulus of shallow rocks down to some depth exceeds the failure shear modulus in (15). The dynamic stress within these rocks exceeds the frictional failure criterion. These rocks crack and thus nonlinearly attenuate energy from the seismic waves. The new cracks (and widened old cracks) reduce the shear modulus for the next strong event and the dynamic stress is not as high. Eventually, the shear modulus approaches that in (15) over the depth range where damage occurs. At that quasi steady state, the few cracks produced by barely reaching frictional failure replace the cracks that closed between seismic events. Damage does not occur at great depth where G_{fail} exceeds the shear modulus of the initial rocks. The shear modulus cannot go all the way to zero at the free surface. This process, called low-cycle fatigue, occurs in engineering applications [*Lubliner*, 1990]. A stiff machine part cracks under imposed strain. There are eventually enough cracks that the part becomes elastically compliant during subsequent strains.

The rocks at the Pilot Hole are suitable for appraising this method. The granite at Parkfield initially began its life as a stiff crystalline rock and was later fractured. The sandstone was buried, likely became stiff, and was exhumed and then fractured [*Blythe et al.*, 2004]. Well logs are available for the granite [*Boness and Zoback*, 2004] and the sandstone [*Ryberg et al.*, 2012] in the Pilot Hole (Figure 4). *Zhang et al.* [2009] and *Ryberg et al.* [2012] estimated the S wave velocity near the Pilot Hole with lower resolution by inverting the results of seismic surveys, including earthquake data.

The inversions did not adequately resolve the S wave in the uppermost 200 m and hence the curvature implied by the predicted curve (16). The shallow S wave velocity of 326 m s^{-1} at the nearby UPSAR array [*Fischer et al.*, 2008b] provides some information. The shallow rocks at the array failed in small earthquakes during the 2004 main shock [*Fischer et al.*, 2008b; *Fischer and Sammis*, 2009]. They thus meet the criterion of being cracked rocks that fail during strong shaking.

The observed S wave velocity in (16) increases with the square root of depth if self-organization has in fact occurred (Figure 4). (I plot this parameter rather than shear modulus, as the seismic inversions did not obtain density at shallow depths and as density is not expected to vary greatly.) The S wave velocity in the sandstone does increase with depth in the expected manner within resolution. I estimate past peak ground velocity from (16), solve for V_D. A calibration point from the plotted curve is 1850 m s^{-1} at 700 m depth. I use of 2300 kg m^{-3} as a generic density for sandstone and retain the starting coefficient of friction of 0.8.

An appropriate velocity c for the near-field pulse is not obvious. I use the typical S wave velocity of the underlying granite of 3000 m s^{-1} [*Boness and Zoback*, 2004] and the phase velocity of generic basin Love waves of 1500 m s^{-1} to provide examples. The estimated past PGV is 2.72 and 1.36 m s^{-1}, respectively. This result is compatible with the inference from the relaxation of ambient stress that strong seismic waves (PGV of ~2 m s^{-1}) impinged on the Pilot Hole site.

The measured S wave velocity within the deepest sandstone is lower (~2000 m s^{-1}) than that of the immediately underlying granite (~3000 m s^{-1}), rather than following the relationship in (14) (Figure 4). The square root of depth curve (16) fit to the sandstone data thus cannot fit the uppermost granite data. The plotted curve does return to the deeper granite data. Qualitatively, I obtained the approximation in (16) by assuming that the near-field pulse imposes the same dynamic strain independent of depth on the inference that deep stiff rocks control the effective phase velocity and the particle velocity. The granite in the Pilot Hole is the stiff underlying rock, so this approximation is likely to be imprecise. Furthermore, the structure of the site is more complicated than the laterally homogeneous medium assumed in (16). In particular, sandstone occurs eastward between the granite of the Pilot Hole and the main fault [e.g., *Zhang et al.*, 2009]. Horizontally propagating S waves from the fault plane will tend to maintain dynamic stress rather than dynamic strain at the vertical sandstone-granite interface. More precise estimates of dynamic stress and strain, predicted stress relaxation, and predicted rock damage might be obtained from three-dimensional numerical models that included realistic seismic waves generated by San Andreas Fault. *Gallovič et al.* [2010] performed linear three-dimensional calculations for the 2004 Parkfield main shock, but did not extract dynamic stress and strain at depth.

A further complication is that crack formation decreases the stiffness and shear wave velocity of the rock mass. This effect should be included in coseismic numerical models. The coseismic S wave velocity to may be ~20% less than the velocity decades after the event [*Sleep and Erickson*, 2014]. However, the S wave velocity increases logarithmically with time after rock failure. The change after the first decade to the next
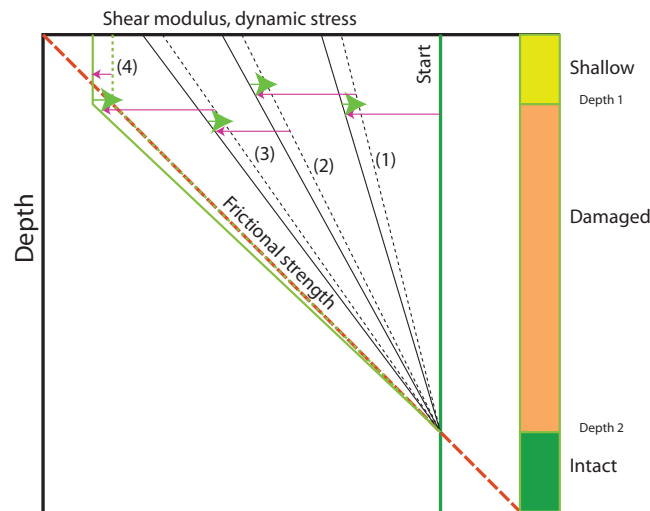
Figure 7. Schematic diagram of the evolution of shear modulus with depth over repeated seismic events. For simplicity, the dynamic strain is the same in all the events so dynamic stress is proportional to the shear modulus. The frictional failure stress increases linearly with depth from the surface. Material starts with the shear modulus of intact rock all the way to the surface. The first event causes failure down to depth 2. The shear modulus decreases to solid line 1 (for simplicity linear with depth). The material heals interseismically to dashed line 1. The next event reduces shear modulus to solid line 2 and healing occurs to dashed line 2. The third event further reduces the shear modulus. The fourth event reduces shear modulus to the frictional strength. The shear modulus increases by healing to frictional strength between events and falls slightly below frictional strength during events. The shear modulus cannot go all the way to zero above depth 1 and damage does not occur below depth 2.

earthquake is only a few percent. My estimates of past PGV did not use S wave velocity estimates to this precision.

5. Application to Whittier Narrows

Strong seismic waves from events on the San Andreas Fault impinge on Downtown Los Angeles. Observation of nearby moderate strong events indicates 3–4 s period Love waves approximately represent shaking within Greater Los Angeles sedimentary basins [*Joyner*, 2000]. Numerical studies show that these waves from northward propagating events pass through Whittier Narrows with high amplitudes [*Graves*, 1996; *Olsen et al.*, 2006; *Graves et al.*, 2008, 2011; *Roten et al.* 2014]. The dynamic stresses in the upper several hundred meters beneath Whittier Narrows exceed frictional failure causing nonlinear attenuation. This process limits the PGV of waves that can propagate into Downtown Los Angeles [*Roten et al.*, 2014; *Sleep and Erickson*, 2014].

Roten et al. [2014] included ambient tectonic stress in their calculations, including for rocks beneath Whittier Narrows. It is relevant to apply (9) to appraise this assumption, as geophysicists have not measured tectonic stress in these rocks. As in the Parkfield area, strike-slip faults and folds above blind-thrust faults accommodate deformation [*Yeats*, 2004; *Meigs et al.*, 2008; *Marshall et al.*, 2009; *Yang and Haukson*, 2011]. The compressional strain rate $\varepsilon'_{\text{tect}}$ is approximately 10^{-7} yr^{-1} [*Marshall et al.*, 2009] (~1 mm yr^{-1} over 10 km across strike). The phase velocity of Love waves is approximately 1500 m s^{-1}. So PGV of 1.5 m s^{-1} produces dynamic strains of ~10^{-3}; the anelastic strains $\varepsilon_{\text{fail}}$ are comparable if frictional failure occurs. The recurrence time t_{quake} of strong shaking is ~100 yr. Thus, $\varepsilon_{\text{fail}}/t_{\text{quake}} \approx 100\varepsilon'_{\text{tect}}$. That is, the model predicts that ambient tectonic stresses are essentially relaxed in the shallow subsurface beneath Whittier Narrows where strong seismic waves are inferred to frequently cause frictional failure. Measurement of ambient stresses at Whittier Narrows would test this hypothesis.

6. Conclusions

Ambient tectonic stress within the shallow subsurface provides potential a class of fragile geological features that are sensitive to relatively infrequent strong seismic waves. The physics are relatively simple in the shallow subsurface. Strong seismic shaking leads to frictional failure within pervasively cracked rock masses. Slip on cracks leads to distributed coseismic strain within the rock mass. Failure that relaxes the ambient tectonic stress is favored, diminishing ambient stress over repeated events. The region of the rock mass with relaxed ambient stress persists until slow deformation (for example, within underlying strong, deep rocks) restores it. Tectonic stress relaxes when dynamic strain divided by earthquake recurrence time exceeds controls the long-term rate of shallow tectonic deformation.

Measurements of ambient tectonic stress are not commonly available for sites within shallow rock where strong shaking is likely. The Pilot Hole at Parkfield near the San Andreas provides a somewhat complicated example where stress relaxation is likely. The regional stress associated away from the weak main fault is

fault-normal compression. This stress is in fact observed deep in the borehole and laterally further away from the fault. The stress in the granite within the borehole between 768 and $\sim$1000–1600 m depth has an orientation appropriate for strike slip. Kinematically, slip on the main fault can restore strike-slip stress much faster than deep horizontal compression beneath the Pilot Hole can restore fault-normal compression. Shear waves with a particle velocity greater than $\sim$2 m s^{-1} would damage the granite above 1000–1600 m depth.

In addition, the ambient sandstone above 768 m depth provides another fragile geological feature. Repeated strong near-field velocity pulses have cracked the sandstone reducing its rigidity. The sandstone has self-organized by low-cycle fatigue so that the typically imposed level of dynamic strain barely produces enough dynamic stress for frictional failure. The S wave velocity then increases with the square root of depth (16). The observed increase of S wave velocity with depth indicates that strong seismic waves with PGV of $\sim$2 m s^{-1} impinged on the site, but the appropriate phase velocity of these waves is not evident without numerical modeling. Both the stress relaxation and S wave velocity results indicate that the Parkfield segment participated in large events (magnitude >7.5, several meter slip) with segments to the south and perhaps even with segments within the creeping zone to the north.

Given the lack of available shallow ambient stress measurements, the question arises whether ambient stress should be included in nonlinear numerical models of strong seismic shaking [*Roten et al.*, 2014]. Whittier Narrows provides an example where Love waves from San Andreas events likely cause nonlinear behavior. If this inference is in fact correct, crack failure from strong shaking is likely to relax tectonic stress faster than it can be restored by deformation at greater depths.

Roten et al. [2014] also included ambient stresses deep within the seismogenic zone. Strong seismic waves result in deep near-fault nonlinear behavior. Self-consistent numerical models of numerous events would allow near-fault ambient stresses to self-organize. *Ma* [2008] calculated such models for single events within simple geological structure.

Appendix A: Ambient Stress Recovery Within the Lithosphere

I present a simple model of stress recovery within the lithosphere using Figure 6, applicable to the case of shallow stress relaxation. The stress resultant is the sum of stresses within the frictional layer and the ductile layer at steady state,

$$\Theta_{ss} = \frac{1}{2}\rho g \mu Z_{max}^2 + \rho g \mu Z_{max} Z_\eta, \tag{A1}$$

where the density ρ and the effective coefficient are for simplicity constant. The peak stress at depth Z_{max} is $\rho g \mu Z_{max}$. The stress in the ductile layer decreases exponentially with depth on the length scale of Z_η. The maximum stress depth increases to depth Z_{new} after the relaxation of stress. The stress in Figure 6 is at friction failure from down to depth Z_T and at $\rho g \mu Z_T$ between Z_T and Z_R. The new stress resultant is

$$\Theta_{new} = \frac{1}{2}\rho g \mu Z_T^2 + \rho g \mu Z_T (Z_R - Z_T) + \frac{1}{2}\rho g \mu Z_{new}^2 - \frac{1}{2}\rho g \mu Z_R^2 + \rho g \mu Z_{new} Z_\eta. \tag{A2}$$

Plate-wide forces control the stress resultant, so $\Theta_{new} = \Theta_{ss}$, which results in a quadratic equation for Θ_{new}.

For simplicity, the strain rate in the ductile region depends on some power N stress at a given depth. The new strain rate is

$$\varepsilon' = \varepsilon'_{ss} \left(\frac{Z_{new}}{Z_{ss}} \right)^N, \tag{A3}$$

where ε'_{ss} is the steady state creep rate. The change of stress between depths Z_T and Z_R, is $E\varepsilon'$, where E is the appropriate elastic modulus. The rate of increase, $\partial Z_T/\partial t$, to the base of the upper fictional zone is

$$\frac{\partial Z_T}{\partial t} = \frac{E\varepsilon'}{\rho g \mu}. \tag{A4}$$

The kinematic time scale to restore the stress at depth Z_R is $t_k \equiv \rho g \mu Z_R / \varepsilon'_{ss} E$. Expressing (A4) with this quantity yields a dimensionless equation,

$$\frac{t_k \partial Z_T}{Z_R \partial t} = \frac{\varepsilon'}{\varepsilon'_{ss}}. \tag{A5}$$

Solving (A2) with $Z_T = 0$ yields the initial strain rate. It is modestly faster than the steady state strain rate for reasonable values of $Z_R/Z_{\max}$, $Z_\eta/Z_{\max}$, and N. The kinematic time scale suffices for purposes of this paper.

References

Anderson, J. G. (2010), Source and site characteristics of earthquakes that have caused exceptional ground accelerations and velocities, *Bull. Seismol. Soc. Am.*, 100, 1–36.

Anderson, J. G., J. N. Brune, J. J. K. Daemen, and M. Purvance (2008), Final report: Task 22—Extreme ground motion studies (2008), *Publ. (YM), Pap. 44*, University of Nevada, Las Vegas, Nev.

Anderson, J. G., J. N. Brune, G. Biasi, A. Anooshehpoor, and M. Pruvance (2011), Workshop report: Applications of precarious rocks and related fragile geological features to US National Hazard Maps, *Seismol. Res. Lett.*, 82(3), 431–441, doi:10.1785/gssrl.82.3.431.

Andrews, D. J., T. C. Hanks, and J. W. Whitney (2007), Physical limits on ground motion at Yucca Mountain, *Bull. Seismol. Soc. Am.*, 97(6) 1771–1792, doi:10.1785/0120070014.

Aoi, S., T. Kunugi, and H. Fujiwara (2008), Trampoline effect in extreme ground motions, *Science*, 332, 727–730.

Bakun-Mazor, D., Y. H. Hatzor, S. D. Glaser, and J. C. Santamarina (2013), Thermally vs. seismically induced block displacements in Masada rock slopes, *Int. J. Rock Mech. Min. Sci.*, 61, 196–211.

Barber, J. R. (2011), Frictional systems subjected to oscillating loads, *Ann. Solid Struct. Mech.*, 2, 45–55.

Barber, J. R., and Y. J. Ahn (2013), Discrete Coulomb frictional systems subjected to periodic loading, in *Recent Advances in Contact Mechanics, LNACM*, vol. 56, edited by G. E. Stavroulakis, pp. 1–11, Springer, Berlin.

Beeler, N. M., T. E. Tullis, and D. L. Goldsby (2008), Constitutive relationships and physical basis of fault strength due to flash heating, *J. Geophys. Res.*, 113, B01401, doi:10.1029/2007JB004988.

Bennington, N., C. Thurber, K. L. Fiegl, and J. Murray-Moraleda (2011), Aftershock distribution as a constraint on the geodetic model of coseismic slip for the 2004 Parkfield earthquake, *Pure Appl. Geophys.*, 168, 1553–1565.

Blythe, A. E., M. A. d'Alessio, and R. Bürgmann (2004), Constraining the exhumation and burial history of the SAFOD pilot hole with apatite fission track and (U-Th)/He thermochronometry, *Geophys. Res. Lett.*, 31, L15S16, doi:10.1029/2003GL019407.

Boness, N. L., and M. D. Zoback (2004), Stress-induced seismic velocity anisotropy and physical properties in the SAFOD Pilot Hole in Parkfield, CA, *Geophys. Res. Lett.*, 31, L15S17, doi:10.1029/2003GL019020.

Boness, N. L., and M. D. Zoback (2006a), A multiscale study of the mechanisms controlling shear velocity anisotropy in the San Andreas Fault Observatory at Depth, *Geophysics*, 71, F131–F146, doi:10.1190/1.2231107.

Boness, N. L., and M. D. Zoback (2006b), Mapping stress and structurally controlled crustal shear velocity anisotropy in California, *Geology*, 34, 825–828, doi:10.1130/G22309.1.

Brudy, M., M. D. Zoback, K. Fuchs, F. Rummel, and J. Baumgärtner (1997), Estimation of the complete stress tensor to 8 km depth in the KTB scientific drill holes: Implications for crustal strength, *J. Geophys. Res.*, 102, 18,453–18,475.

Brune, J. N. (2001), Shattered rock and precarious rock evidence for strong asymmetry in ground motions during thrust faulting, *Bull. Seismol. Soc. Am.*, 91(3), 441–447.

Chéry, J., M. D. Zoback, and S. Hickman (2004), A mechanical model of the San Andreas Fault and SAFOD Pilot Hole stress measurements, *Geophys. Res. Lett.*, 31, L15S13, doi:10.1029/2004GL019521.

Day-Lewis, A., M. Zoback, and S. Hickman (2010), Scale invariant stress orientations and seismicity rates near the San Andreas Fault, *Geophys. Res. Lett.*, 37, L24304, doi:10.1029/2010GL045025.

Dieterich, J. H. (1979), Modeling of rock friction. 1: Experimental results and constitutive equations, *J. Geophys. Res.*, 84, 2161–2168.

Drucker, D. C., and W. Prager (1952), Soil mechanics and plastic analysis or limit design, *Q. Appl. Math.*, 10, 157–165.

Dunham, E. M., D. Belanger, L. Cong, and J. E. Kozdon (2011a), Earthquake ruptures with strongly rate-weakening friction and off-fault plasticity. 1: Planar faults, *Bull. Seismol. Soc. Am.*, 101(5), 2296–2307, doi:10.1785/0120100075.

Dunham, E. M., D. Belanger, L. Cong, and J. E. Kozdon (2011b), Earthquake ruptures with strongly rate-weakening friction and off-fault plasticity. 2: Nonplanar faults, *Bull. Seismol. Soc. Am.*, 101(5), 2308–2322, doi:10.1785/0120100076.

Ellsworth, W. L., M. Celebi, J. R. Evans, E. G. Jensen, R. Kayen, M. C. Metz, D. J. Nyman, J. W. Roddick, P. Spudich, and C. D. Stephens (2004), Near-Field ground motion of the 2002 Denali Fault, Alaska, Earthquake Recorded at Pump Station 10, *Earthquake Spectra*, 20(3), 597–615.

Fischer, A. D., and C. G. Sammis (2009), Dynamic driving of small shallow events during strong motion, *Bull. Seismol. Soc. Am.*, 99, 1720–1729.

Fischer, A. D., C. G. Sammis, Y. L. Chen, and T.-L. Teng (2008a), Dynamic triggering by strong motion P- and S-waves: Evidence from 1999 Chi-Chi, Taiwan Earthquake, *Bull. Seismol. Soc. Am.*, 98, 580–592.

Fischer, A. D., Z. G. Peng, and C. G. Sammis, (2008b), Dynamic triggering of high-frequency bursts by strong motions during the 2004 Parkfield earthquake sequence, *Geophys. Res. Lett.*, 35, L12305, doi:10.1029/2008GL033905.

Gallovič, F., M. Käser, J. Burjánek, and C. Papaioannou (2010), Three-dimensional modeling of near-fault ground motions with nonplanar rupture models and topography: Case of the 2004 Parkfield earthquake, *J. Geophys. Res.*, 115, B03308, doi:10.1029/2008JB006171.

Graves, R. (1996), Simulating seismic wave propagation in 3D elastic media using staggered grid finite differences, *Bull. Seismol. Soc. Am.*, 86, 1091–1106.

Graves, R. W., B. T. Aagaard, K. W. Hudnut, L. M. Star, J. P. Stewart, and T. H. Jordan (2008), Broadband simulations for Mw7.8 southern San Andreas earthquakes: Ground motion sensitivity to rupture speed, *Geophys. Res. Lett.*, 35, L22302, doi:10.1029/2008GL035750.

Graves, R. W., B. T. Aagaard, and K. W. Hudnut (2011), The ShakeOut earthquake source and ground motion simulations, *Earthquake Spectra*, 27, 273–291, doi:10.1193/1.3570677.

Hanks, T. C., N. A. Abrahamson, M. Board, D. M. Boore, J. N. Brune, and C. A. Cornell (Eds.) (2006), Report of the workshop on extreme ground motions at Yucca Mountain, August 23–25, 2004, *Open File Rep., 2006-1277*, 234 pp., U. S. Geol. Survey, Reston, Va.

Hickman, S., and M. Zoback (2004), Stress orientations and magnitudes in the SAFOD Pilot Hole: Implications for the strength of the San Andreas fault at Parkfield, *Geophys. Res. Lett.*, 31, L15S12, doi:10.1029/2004GL020043.

Hill, D. P. (2008), Dynamic stresses, Coulomb failure, and remote triggering, *Bull. Seismol. Soc. Am.*, 98(1), 66–92, doi:10.1785/0120070049.

Housner, A. W., and M. O. Trifunac (1967), Analysis of accelerograms-Parkfield earthquake, *Bull. Seismol. Soc. Am.*, 57, 1193–1220.

Jana, P., and A. Chatterjee (2013), Modal damping in vibrating objects *via* dissipation from dispersed frictional microcracks, *Proc. R. Soc. A*, *469*, 20120685.

Joyner, W. B. (2000), Strong motion from surface waves in deep sedimentary basins, *Bull. Seismol. Soc. Am.*, *90*(6B), S95–S112.

Linker, M. F., and J. H. Dieterich (1992), Effects of variable normal traction on rock friction: Observations and constitutive equations, *J. Geophys. Res.*, *97*, 4923–4940.

Lubliner, J. (1990), *Plasticity Theory*, 495 pp., Macmillan, N. Y.

Ma, S. (2008), A physical model for widespread near-surface and fault zone damage induced by earthquakes, *Geochem. Geophys. Geosyst.*, *9*, Q11009, doi:10.1029/2008GC002231.

Marsan D. (2005), The role of small earthquakes in redistributing crustal elastic stress, *Geophys. J. Int.*, *163*, 141–151.

Marshall, S. T., M. L. Cooke, and S. E. Owen (2009), Interseismic deformation associated with three-dimensional faults in the greater Los Angeles region, California, *J. Geophys. Res.*, *114*, B12403, doi:10.1029/2009JB006439.

McCalpin, J. P., and E. W. Hart (2003), Ridge-top spreading features and relationship to earthquakes, San Gabriel Mountains Region. Part B: Paleoseismic investigations of ridgetop depressions, in *Ridge-Top Spreading in California, California Geol. Surv. Open File Rep. 1*, edited by E. W. Hart, Contrib. 4, 51 pp., CD-ROM, Sacramento, Calif.

Meigs, A. J., M. L. Cooke, and S. T. Marshall (2008), Using vertical rock uplift patterns to constrain the three-dimensional fault configuration in the Los Angeles Basin, *Bull. Seismol. Soc. Am.*, *98*(2) 106–123.

Nakata, N., and R. Snieder (2011), Near-surface weakening in Japan after the 2011 Tohoku-Oki earthquake, *Geophys. Res. Lett.*, *38*, L17302, doi:10.1029/2011GL048800.

Nakata, N., and R. Snieder (2012a), Estimating near-surface shear wave velocities in Japan by applying seismic interferometry to KiK-net data, *J. Geophys. Res.*, *117*, B01308, doi:10.1029/2011JB008595.

Nakata, N., and R. Snieder (2012b), Time-lapse change in anisotropy in Japan's near surface after the 2011 Tohoku-Oki earthquake, *Geophys. Res. Lett.*, *39*, L11313, doi:10.1029/2012GL051979.

Noda, H., E. M. Dunham, and J. R. Rice (2009), Earthquake ruptures with thermal weakening and the operation of major faults at low overall stress levels, *J. Geophys. Res.*, *114*, B07302, doi:10.1029/2008JB006143.

Olsen, K. B., S. M. Day, J. B. Minster, Y. Cui, A. Chourasia, M. Faerman, R. Moore, P. Maechling, and T. Jordan (2006), Strong shaking in Los Angeles expected from southern San Andreas earthquake. *Geophys. Res. Lett.*, *33*, L07305, doi:10.1029/2005GL025472.

Page, B. M., R. G. Coleman, and G. A. Thompson (1998), Late Cenozoic tectonics of the central and southern Coast Ranges of California, *Geol. Soc. Am. Bull.*, *110*(7), 846–876.

Roten, D., K. B. Olsen, S. Day, Y. Cui, and D. Fäh (2014), Expected seismic shaking in Los Angeles reduced by San Andreas Fault zone plasticity, *Geophys. Res. Lett.*, *41*, 2769–2777, doi:10.1002/2014GL059411.

Ruina, A. (1980), Friction laws and instabilities: A quasistatic analysis of some dry frictional material, PhD thesis, 99 pp., Brown Univ., Providence, R. I.

Ruina, A. (1983), Slip instability and state variable laws, *J. Geophys. Res.*, *88*, 10,359–10,370.

Ryberg, T., J. A. Hole, G. S. Fuis, M. J. Rymer, F. Bleibinhaus, D. Stromeyer, and K. Bauer (2012), Tomographic V_p and V_s structure of the California Central Coast Ranges, in the vicinity of SAFOD, from controlled-source seismic data, *Geophys. J. Int.*, *190*, 1341–1360.

Sawazaki, K., and R. Snieder (2013), Time-lapse changes of *P*- and *S*-wave velocities and shear wave splitting in the first year after the 2011 Tohoku earthquake, Japan: Shallow subsurface, *Geophys. J. Int.*, *193*, 238–251.

Shakal, A., H. Haddadi, V. Graizer, K. Lin, and M. Huang (2006), Some key features of the strong-motion data from the M6.0 Parkfield, California, earthquake of 28 September 2004, *Bull. Seismol. Soc. Am.*, *96*(4B), S90–S118.

Sleep, N. H. (2010), Strong seismic shaking of randomly prestressed brittle rocks, rock damage, and nonlinear attenuation, *Geochem. Geophys. Geosyst.*, *11*, Q10002, doi:10.1029/2010GC003229.

Sleep, N. H. (2011a), Deep-seated downslope slip during strong seismic shaking, *Geochem. Geophys. Geosyst.*, *12*, Q12001, doi:10.1029/2011GC003838.

Sleep, N. H. (2011b), Seismically damaged regolith as self-organized fragile geological feature, *Geochem. Geophys. Geosyst.*, *12*, Q12013, doi:10.1029/2011GC003837.

Sleep, N. H. (2012), Microscopic elasticity and rate and state friction evolution laws, *Geochem. Geophys. Geosyst.*, *13*, Q12002, doi:10.1029/2012GC004393.

Sleep, N. H., and B. A. Erickson (2014), Nonlinear attenuation of S-waves and Love waves within ambient rock, *Geochem. Geophys. Geosyst.*, *15*, 1419–1440, doi:10.1002/2014GC005250.

Sleep, N. H., and P. Hagin (2008), Nonlinear attenuation and rock damage during strong seismic ground motions, *Geochem. Geophys. Geosyst.*, *9*, Q10015, doi:10.1029/2008GC002045.

Sleep, N. H., and S. Ma (2008), Production of brief extreme ground acceleration pulses by nonlinear mechanisms in the shallow subsurface, *Geochem. Geophys. Geosyst.*, *9*, Q03008, doi:10.1029/2007GC001863.

Sleep, N. H., and M. D. Zoback (2007), Did earthquakes keep the early crust habitable?, *Astrobiology*, *7*, 1023–1032.

Townend, J., and M. D. Zoback (2000), How faulting keeps the crust strong, *Geology*, *28*, 399–402.

Townend, J., and M. D. Zoback (2004), Regional tectonic stress near the San Andreas Fault in central and southern California, *Geophys. Res. Lett.*, *31*, L15S11, doi:10.1029/2003GL018918.

Turcotte, D. L., and G. Schubert (2002), *Geodynamics*, 2nd ed., 456 pp., John Wiley, N. Y.

Yang, W., and E. Hauksson (2011), Evidence for vertical partitioning of strike-slip and compressional tectonics from seismicity, focal mechanisms, and stress drops in the East Los Angeles Basin area, California, *Bull. Seismol. Soc. Am.*, *101*, 964–974.

Yeats, R. S. (2004), Tectonics of the San Gabriel Basin and surroundings, southern California, *Geol. Soc. Am. Bull.*, *116*(9–10), 1158–1182.

Zhang, H., C. Thurber, and P. Bedrosian (2009), Joint inversion for Vp, Vs, and Vp/Vs at SAFOD, Parkfield, California, *Geochem. Geophys. Geosyst.*, *10*, Q11002, doi:10.1029/2009GC002709.

Zoback, M. D., and J. H. Healy (1992), In situ stress measurements to 3.5 km depth in the Cajon Pass Scientific Research Borehole: Implications for the mechanics of crustal faulting, *J. Geophys. Res.*, *97*, 5039–5057, doi:10.1029/91JB02175.

Zoback, M. D., and J. Townend (2001), Implications of hydrostatic pore pressures and high crustal strength for the deformation of intraplate lithosphere, *Tectonophysics*, *336*, 19–30.

Zoback, M. D., J. Townend, and B. Grollimund (2002), Steady-state failure equilibrium and deformation of intraplate lithosphere, *Int. Geol. Rev.*, *44*, 383–401.